

Enhancing the Corrosion Resistance of Near-Stoichiometric Ni₄Mo Alloy by Doping with Yttrium

H. M. Tawancy

Received: 19 April 2012 / Accepted: 13 July 2012 / Published online: 2 August 2012
© Springer Science+Business Media, LLC and ASM International 2012

Abstract It is shown that doping with yttrium can significantly improve the corrosion resistance of near-stoichiometric Ni₄Mo alloy, which is otherwise susceptible to severe intergranular attack in the ordered condition. A one-to-one correspondence is found to exist between corrosion resistance and morphology of ordered Ni₄Mo. The susceptibility to intergranular corrosion is correlated with a discontinuous grain boundary reaction resulting from self-generated recrystallization to accommodate the strain associated with continued growth of the ordered crystals. Doping with Y is found to maintain an ultrafine ordered microstructure suppressing the occurrence of self-generated recrystallization and, therefore, improving the corrosion resistance.

Keywords Optical microscopy · Intermetallics · Corrosion testing · Electron microscopy

Introduction

Nickel–molybdenum alloys containing more than 25 wt.% Mo have been of particular importance to the chemical process industry because of their high corrosion resistance particularly in reducing media such as hydrochloric acid [1, 2]. Experiment shows that Mo has the effect of increasing anodic polarization and, therefore, the corrosion rate of the alloy becomes anodically controlled [2, 3]. However, a drawback of these alloys is their structural instability

during exposure at elevated temperatures such as occurs during thermo-mechanical processing, welding operations, and under certain service conditions. This results from the tendency of these alloys to undergo a disorder-to-order transformation whereby the high-temperature face-centered cubic (fcc) phase is transformed into a D1_a superlattice with tetragonal structure [4, 5]. At the exact stoichiometric composition of Ni₄Mo (Ni-29.1 wt.% Mo) and according to the equilibrium phase diagram, the transformation occurs at temperatures just below about 870 °C [5]. In practice, however, the transformation occurs with rapid kinetics in the vicinity of 700 °C [4, 5].

Earlier studies have shown that long-range ordering to Ni₄Mo could have adverse effects on ductility [4–7] and corrosion resistance [8]. Recently, however, it has been reported that the ductility of Ni₄Mo could be significantly improved by minor but critical additions of yttrium [9, 10]. However, the effect of the addition of yttrium on corrosion resistance is not well understood. In recent years, there has been an increasing interest in using intermetallic compounds and ordered alloys in advanced technological applications because of their potentially useful combination of properties [11, 12]. Therefore, it becomes important to develop a better understanding of the behavior of these materials to improve their performance and extend the range of their applications.

As the characterization of materials both physically and chemically is essential in order for continued progress to be made in understanding materials performance and to improve existing materials, or to develop new materials, this investigation has been carried out with the objective to: (i) a better understanding of how the disorder-to-order transformation in Ni₄Mo alloy influences its corrosion resistance and (ii) develop an anti-corrosion method to expand the scope of applications of alloys in this category.

H. M. Tawancy (✉)
Center for Engineering Research, Research Institute,
King Fahd University of Petroleum & Minerals
KFUPM, P.O. Box 1639, Dhahran 31261, Saudi Arabia
e-mail: tawancy@kfupm.edu.sa

Experimental Procedure

The alloys used in the study were prepared by standard techniques of vacuum induction melting and electro-slag re-melting followed by forging, hot rolling, and then cold rolling to sheets about 1.5 mm in thickness. Table 1 lists the chemical compositions of the two alloys included in the study. Specimens were solution annealed at 1065 °C for 15 min and then water quenched. Thermal aging to induce long-range ordering was carried out at temperatures in the range of 500–900 °C for up to 100 h. Resistance to corrosion was determined from aqueous tests in boiling 20% HCl carried out on sheet specimens (25.4 × 25.4 × 1.5 mm) according to ASTM standard G1-88 [13]. The corrosion rates were determined from the average of three weight loss measurements after 24-h immersion in HCl using the well-known formula: $\text{mpy} = 534 W/DAT$, where mpy refers to corrosion rate in mils/year, W is the measured weight loss in milligram, D is the density of the material, A is the specimen area in square inch, and T is the exposure time in hours. In general, a corrosion rate of ≤ 5 mpy (0.13 mm/year) reflects a high corrosion resistance, a corrosion rate >5 mpy but <50 mpy is considered acceptable, and if it exceeds 50 mpy (1.3 mm/year) it becomes unacceptable [13, 14].

Various techniques used to characterize the microstructure included light optical microscopy, x-ray diffraction, transmission/scanning transmission electron microscopy combined with microchemical analysis by energy dispersive x-ray spectroscopy, and Auger electron spectroscopy using scanning Auger microprobe. Specimens for light optical microscopy were etched in a solution consisting of 80% HCl and 20% of 15 mol chromic acid. X-ray diffraction experiments were carried out on metallographic specimens in the as-polished condition. Thin-foil specimens for transmission electron microscopy were prepared by the jet polishing technique in a solution consisting of 30% nitric acid in methanol. All foils were examined at 200 keV in a microscope equipped with an energy dispersive x-ray spectrometer and a condenser lens system, which focuses the electron beam to 2 nm in diameter. Specimens in the ordered condition for Auger electron spectroscopy were fractured in situ to measure the Mo content of freshly exposed grain boundaries and generate Mo-depth profiles by sputtering thin layers at a rate of 1 nm/min. Because of the closely related crystallographic relationship between

the fcc structure of the parent high-temperature phase of Ni_4Mo and D1_a superlattice, electron diffraction patterns are indexed in terms of the fcc structure.

Experimental Results and Discussion

Figure 1(a) shows the effect of aging time up to 100 h at temperatures in the range of 500–900 °C on the corrosion rate of the Y-free alloy in boiling 20% HCl. It is observed that the corrosion rate increases with aging time more rapidly at 700 °C coinciding with the temperature corresponding to accelerated ordering kinetics [4, 5]. However, after up to 1 h of aging, the corrosion rate is not significantly changed from that in the annealed condition remaining in the vicinity of about 0.35 mm/year (14 mpy).

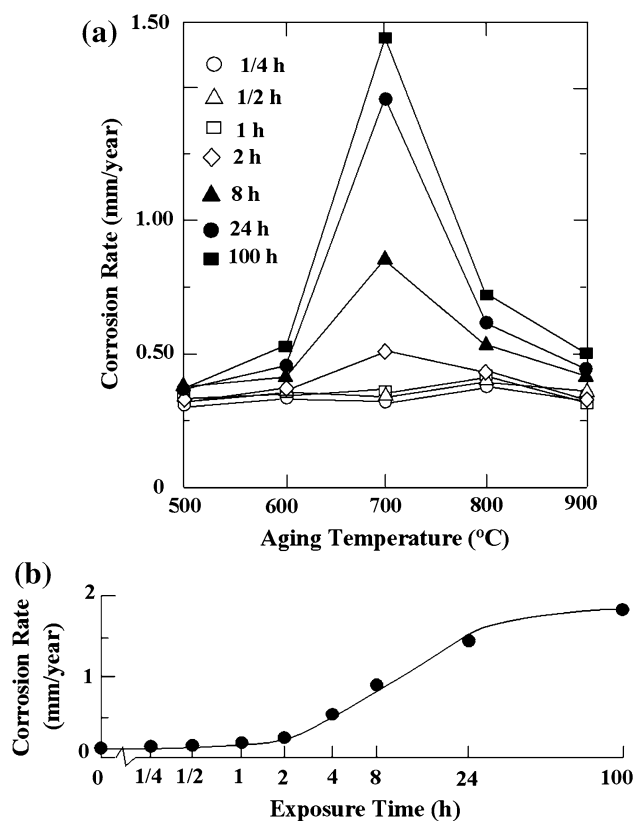


Fig. 1 Corrosion rate of Ni_4Mo alloy in boiling 20% HCl. **a** Functional dependence of corrosion rate on aging time up to 100 h at temperatures in the range of 500–900 °C. **b** Effect of aging time up to 100 h at 700 °C on the corrosion rate

Table 1 Chemical compositions (wt.%)

Ni	Mo	Co	Cr	Fe	Mn	Si	C	S	Y
Balance	28.78	<0.1	<0.1	<0.1	<0.1	<0.02	0.002	<0.002	...
Balance	28.65	<0.1	<0.1	<0.1	<0.1	<0.02	0.002	<0.002	0.009

This is further illustrated in Fig. 1(b) showing the effect of aging time at 700 °C on the corrosion rate. However, with continued aging, it can be seen that the corrosion rate increases at a higher rate reaching about 1.5 mm/year (59 mpy) after 24 h and then increases at a much slower rate with further aging. Corresponding to this behavior, Fig. 2 shows comparative light optical micrographs of corrosion tested specimens. After up to 1 h of aging, corrosion is observed to occur uniformly as illustrated in the light optical micrograph of Fig. 2(a). However, after 24 h of aging, extensive intergranular attack is observed as shown in Fig. 2(b). To understand the origin of this

behavior, detailed microstructural characterization has been carried out as described below.

X-ray diffraction patterns illustrating the structural changes in the Y-free alloy as a function of aging time at 700 °C are shown in Fig. 3(a). In the annealed condition, the material exhibits a diffraction pattern typical of fcc structure as expected. However, diffuse intensity maxima are observed in electron diffraction patterns at $\langle 1 \frac{1}{2} 0 \rangle_{\text{fcc}}$ positions typifying short-range order in annealed Ni–Mo alloys [5, 15–17] as shown in the example of Fig. 3(b). After 1 h of aging, reflections characteristic of the $D1_a$ superlattice of Ni_4Mo (tetragonal structure; $a = 0.572 \text{ nm}$,

Fig. 2 Light optical micrographs of corrosion tested specimens of the Ni_4Mo alloy. Micrograph typical of specimens aged **a** 1 h at 700 °C and **b** 24 h at 700 °C

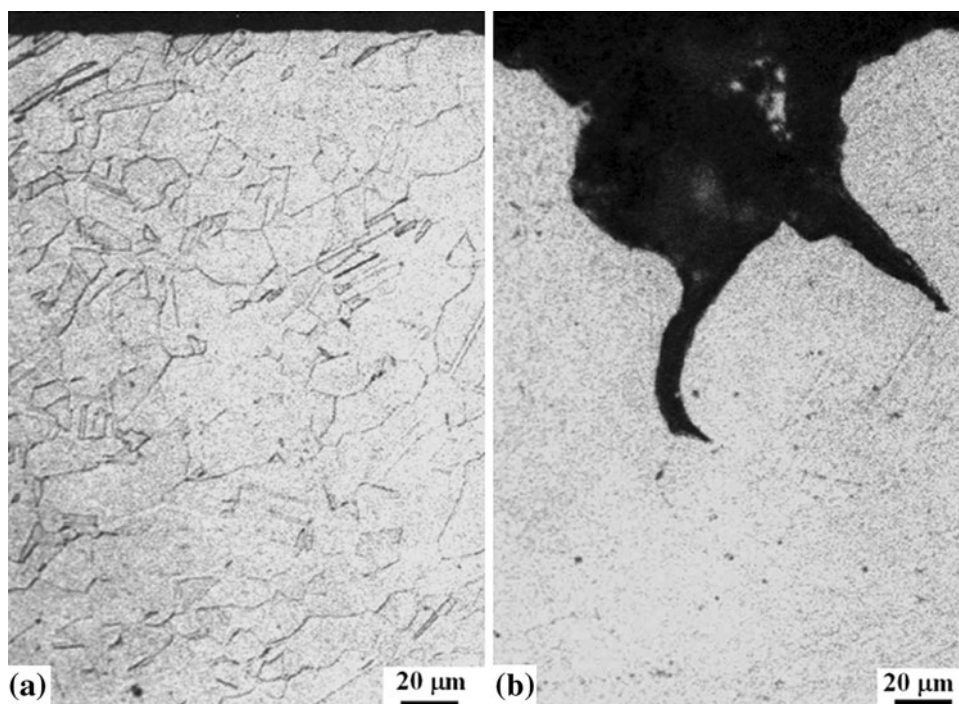
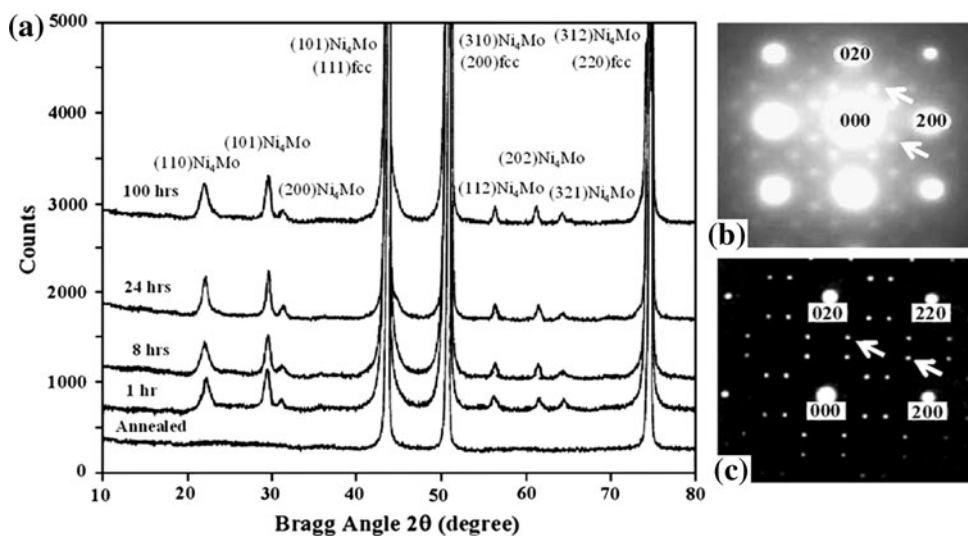


Fig. 3 Structure of the Ni_4Mo alloy as a function of aging time at 700 °C. **a** Effect of aging time up to 100 h at 700 °C on the appearance of x-ray diffraction patterns derived from the surface of polished specimens. **b** $\langle 001 \rangle_{\text{fcc}}$ electron diffraction pattern representative of the annealed condition; short-range order reflections at $\langle 1 \frac{1}{2} 0 \rangle$ positions are indicated by the arrows. **c** $\langle 001 \rangle_{\text{fcc}}$ electron diffraction pattern representative of specimens aged 1–100 h at 700 °C; superlattice reflections of Ni_4Mo at $1/5(420)$ positions are indicated by the arrows



$c = 0.356$ nm) are observed in the x-ray diffraction patterns (Fig. 3a). In the corresponding electron diffraction patterns, the short-range order reflections observed in the annealed condition (Fig. 3b) are replaced by the characteristic $D1_a$ superlattice reflections at $1/5\langle 420 \rangle_{fcc}$ and all equivalent positions as shown in Fig. 3(c). This demonstrates the closely related crystallographic features of the fcc structure and $D1_a$ superlattice in that the $D1_a$ superlattice can directly be derived from the fcc structure by minor atoms rearrangement on $\{420\}_{fcc}$ planes such that every fifth plane becomes occupied by Mo atoms and planes in-between contain only Ni atoms giving rise to the observed superlattice reflections at $1/5\langle 420 \rangle_{fcc}$ positions (Fig. 3c) and a total of six crystallographically equivalent variants of Ni_4Mo crystals. Therefore, for an alloy at or near the stoichiometric composition, diffusion over short distances is only required to establish the $D1_a$ superlattice, which could explain the observed rapid kinetics of the fcc-to- $D1_a$ superlattice transformation at $700^\circ C$.

As can be seen from the x-ray diffraction data of Fig. 3(a), the intensities of the $D1_a$ superlattice reflections developed after 1 h of aging remain essentially unchanged after up to 100 h suggesting that the atomic ordering process for the alloy studied is completed within the first 1 h

of aging at $700^\circ C$. Combining this result with the corrosion data of Fig. 1 suggests that the extensive intergranular attack observed after 24 h of aging (Fig. 2b) is not related to process of atomic order itself. Rather, this behavior is found to be associated with changes in morphology of the ordered microstructure of Ni_4Mo during the later stages of aging as demonstrated below.

Figure 4 shows bright-field transmission electron microscopy images illustrating the evolution of the ordered microstructure in the matrix of the Ni_4Mo alloy during aging at $700^\circ C$. Initially, a mottled contrast characteristic of large volume fraction of ultrafine particles is observed (Fig. 4a). Subsequently, aligned arrays of nanosized particles of Ni_4Mo are distinguished (Fig. 4b). With continued aging, these particles are observed to grow to impingement and ultimately form a mosaic assembly of transformation twins on the $\{100\}_{fcc}$ planes, as shown in Fig. 4(c) and (d). It is to be noted that the diffraction pattern shown in Fig. 3(c) can be interpreted as two twin-related patterns with $\langle 001 \rangle_{fcc}$ as twin axis. Figure 5 shows dark-field TEM images formed with $1/5\langle 420 \rangle_{fcc}$ superlattice reflections to illustrate the effect of aging time at $700^\circ C$ on the morphology of one crystallographic variant of Ni_4Mo . After 1 h of aging corresponding to completion of atomic order,

Fig. 4 Bright-field TEM images illustrating the evolution of the ordered microstructure in the matrix of Ni_4Mo alloy as a function of aging time at $700^\circ C$. **a** 15 min, **b** 1 h, **c** 8 h, and **d** 24 h

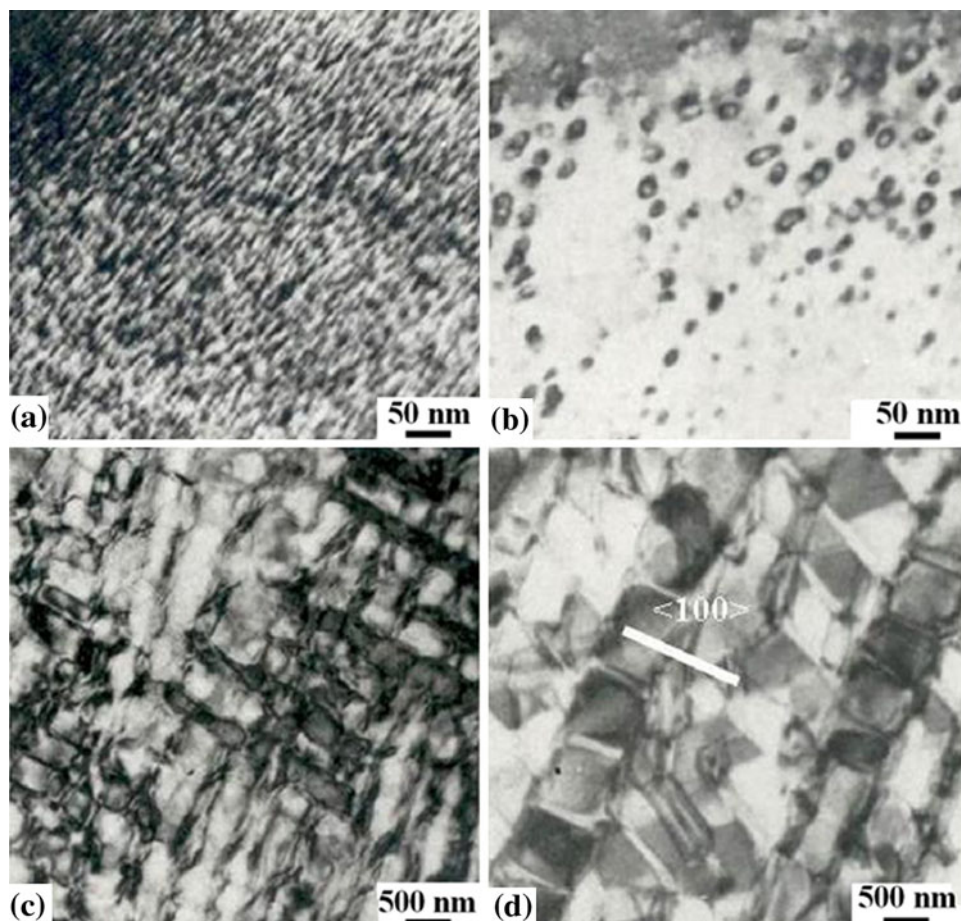
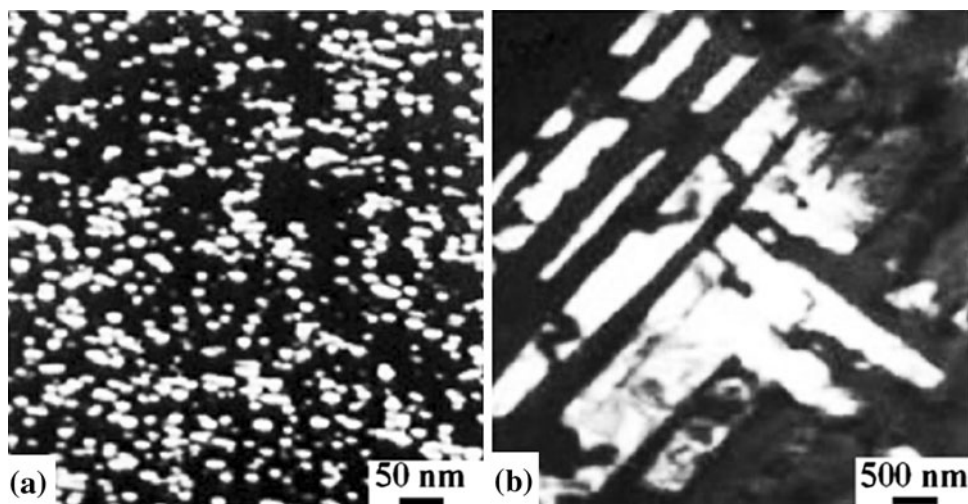


Fig. 5 Effect of aging time at 700 °C on the morphology of Ni₄Mo. **a** Dark-field transmission electron microscopy image formed with $1/5\langle 420 \rangle_{\text{fcc}}$ superlattice reflection and illustrating the morphology of one variant of Ni₄Mo with nanosized crystals (specimen aged 1 h). **b** Dark-field transmission electron microscopy image showing the respective morphology after 100 h of aging; considerable coarsening is noted



Ni₄Mo is observed to assume the morphology of nanosized particles, as shown in Fig. 5(a). However, large platelets of Ni₄Mo are observed during the later stages of exposure as shown in the example of Fig. 5(b) corresponding to 24 h of aging. Associated with this coarsening is the observation of a cellular or lamellar structure of Ni₄Mo at the grain boundaries of the parent fcc structure as shown in the example of Fig. 6 for a specimen aged 100 h at 700 °C. On the scale of light optical microscopy, two distinct morphologies of Ni₄Mo are observed: (i) large platelets of forming a Widmanstatten pattern and (ii) a lamellar structure of at grain boundaries typical of a discontinuous grain boundary reaction as illustrated in Fig. 6(a). An example showing the identification of Ni₄Mo lamellae at a grain boundary by transmission electron microscopy and diffraction is shown Fig. 6(b) and (c). Figure 6(d) and (e) are energy dispersive x-ray spectra showing, respectively, the elemental compositions of the Ni₄Mo lamellae and adjacent matrix region marked x in Fig. 6(b). It is observed that the matrix region is depleted in Mo. This is further confirmed by the results of Auger electron spectroscopy summarized in the Mo-depth profile shown in Fig. 7. The inset is a secondary electron image showing the surface exposed by in situ fracture of a specimen aged for 100 h at 700 °C. In this case, fracture occurs by an intergranular mode [4, 6]. As can be seen, the grain boundary is considerably depleted in Mo consistent with the transmission/scanning electron microscopy results of Fig. 6. As expected, the Mo content increases with distance from grain boundary.

Based upon the above observations, it is possible to correlate the extensive intergranular attack observed in Fig. 2(b) with changes in the morphology of ordered Ni₄Mo with extended aging rather than with atomic order. It is expected that because of the relatively low diffusivity of Mo in Ni [17], the observed Mo-depleted

zones in the vicinity of grain boundaries may exist in a state of metastable equilibrium for extended periods of time.

Changes in morphology of ordered phases after completion of the process of atomic order such as that described above are also observed in other ordered alloy systems such as Ni₃Fe and Ni₂V and have been correlated with self-generated recrystallization to accommodate the build-up of strain associated with growth of the ordered structure [18]. However, in this case, the Y-doped alloy is found to exhibit a different behavior in that the tendency for self-generated recrystallization is considerably decelerated as reflected by the corresponding corrosion behavior summarized in Fig. 8. It is observed that after up to 100 h of aging at 700 °C, the Y-doped alloy maintains a corrosion rate comparable to that observed in the annealed condition as shown in Fig. 8(a). The light optical micrograph of Fig. 8(b) demonstrates that corrosion of the Y-doped alloy in boiling 20% HCl occurs uniformly even after up to 100 h of aging at 700 °C, which can be correlated with the observed distribution of Y throughout the microstructure as shown below.

It is well known that Y has the tendency to segregate at surfaces and various types of interfaces. An example illustrating the ordering behavior of the Y-doped alloy with particular reference to the distribution of Y is shown in Fig. 9. Two distinctive microstructural features are observed in the bright-field scanning transmission electron microscopy image of Fig. 9(a): (i) the discontinuous ordering transformation at the grain boundary is suppressed and (ii) the ordered crystals of Ni₄Mo within the matrix maintain the ultrafine structure observed after short-term exposure of the Y-free alloy (Figs. 4, 5). Figure 9(b) shows the concentration profile of Y across the grain boundary of Fig. 9(a) as determined by point analysis in the scanning transmission electron microscopy mode using a 2 nm probe

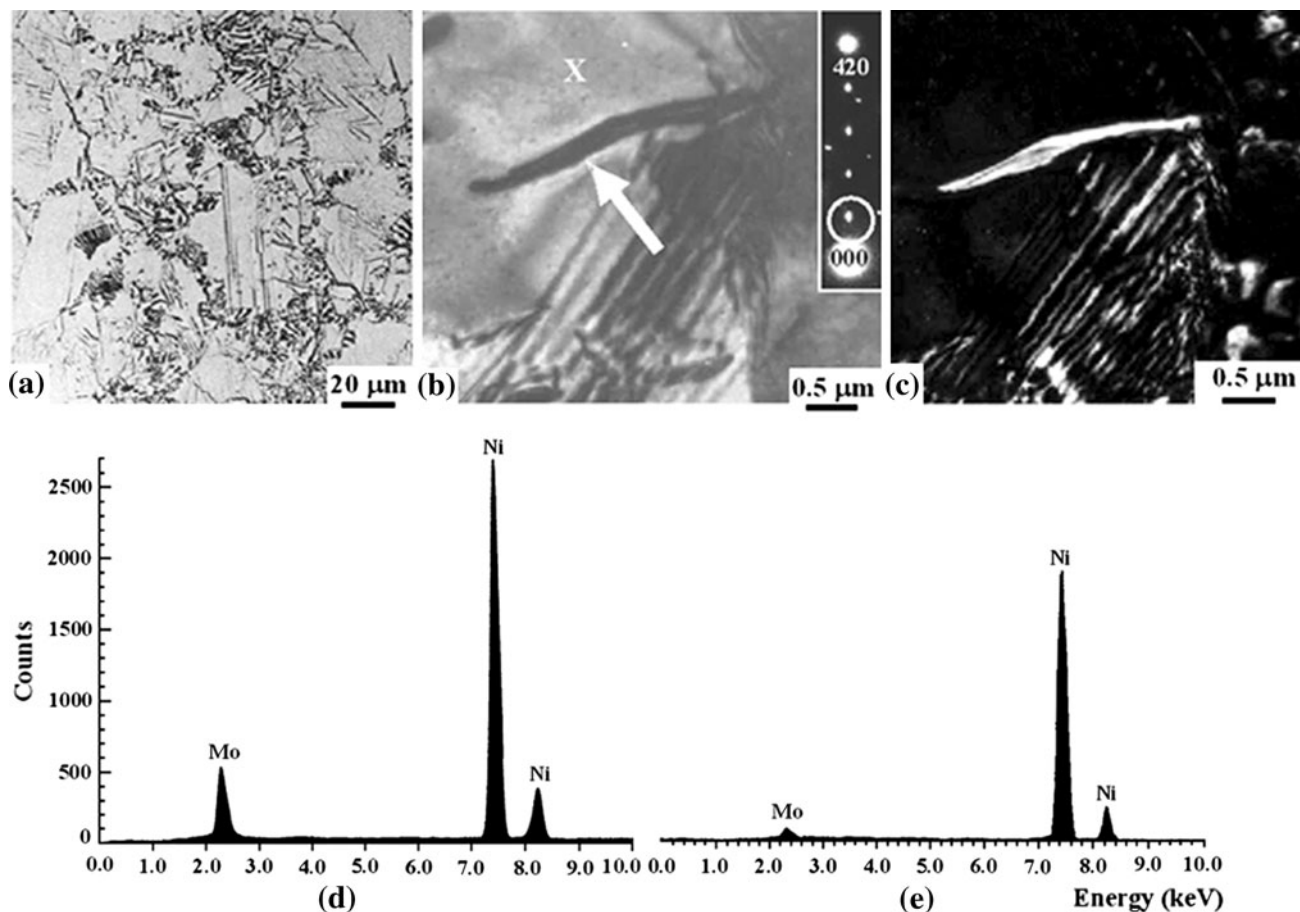


Fig. 6 An example illustrating the formation of Ni_4Mo with lamellar structure by discontinuous reaction at grain boundaries of the parent high-temperature phase (specimen aged 100 h at 700 °C). **a** Light optical micrograph showing the gross microstructural features, **b** bright-field transmission electron microscopy image showing a lamellae of Ni_4Mo indicated by the arrow; the inset is corresponding

diffraction pattern, **c** corresponding dark-field image formed with the encircled $1/5(420)_{\text{fcc}}$ superlattice reflection in the inset of **(b)**. **d** Energy dispersive x-ray spectrum showing the elemental composition of the Ni_4Mo lamellae. **e** Energy dispersive x-ray spectrum showing the elemental composition of the matrix region marked **x** in **b**

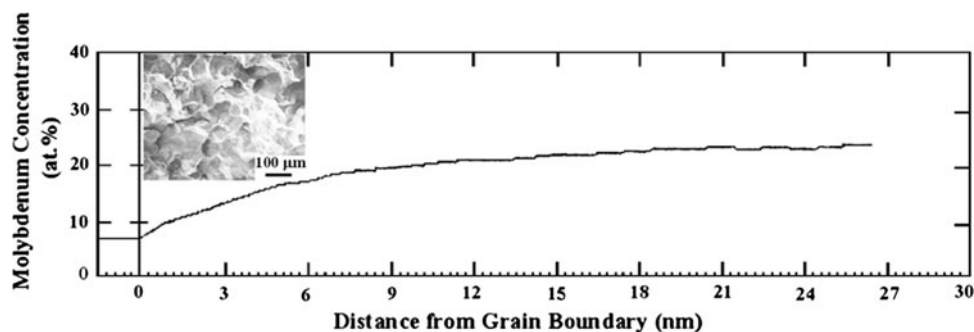


Fig. 7 Depth profile of Mo derived from the Ni_4Mo alloy in the ordered condition by Auger electron spectroscopy illustrating the concentration of Mo as a function of distance from grain boundary

(specimen aged 100 h at 700 °C and then in situ fractured to analyze freshly exposed grain boundaries shown in the secondary electron image of the inset)

diameter. Although some Y is present within the grains, it exhibits a greater tendency to segregate at grain boundaries. It is also possible that Y within the grains is

segregated at the interfaces separating the ordered crystals maintaining an ultrafine structure. Therefore, most evidence points out that Y has the effect of stabilizing the

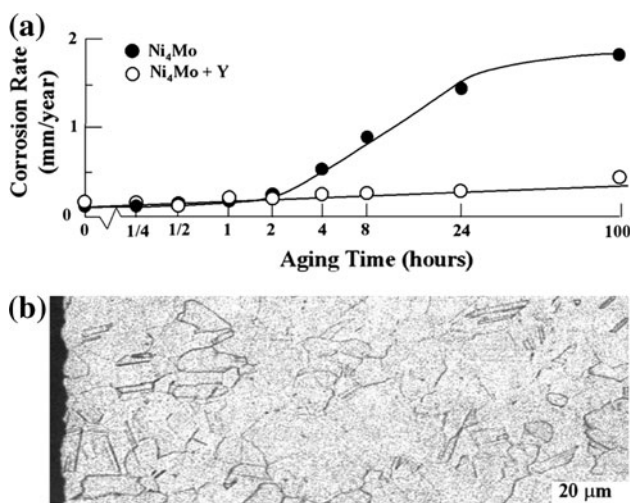


Fig. 8 Effect of doping with Y on the corrosion behavior of Ni₄Mo alloy. **a** Comparative corrosion rates of the Ni₄Mo and Ni₄Mo + Y alloys as functions of aging time at 700 °C. **b** Light optical micrograph of corrosion tested specimen of the Y-doped alloy after 24 h of aging at 700 °C

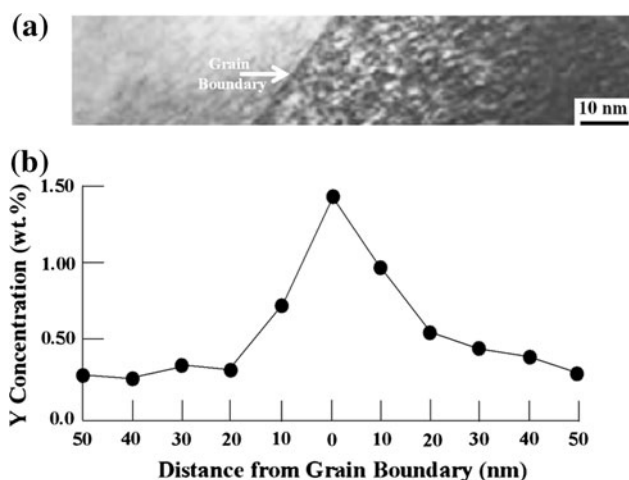


Fig. 9 Ordering behavior of the Y-doped Ni₄Mo alloy. **a** Bright-field scanning transmission electron microscopy image showing a grain boundary of a specimen aged 100 h at 700 °C. **b** Corresponding concentration profile of Y across the grain boundary shown in (a)

ultrafine ordered microstructure suppressing the occurrence of self-generated recrystallization after at least 100 h of aging at 700 °C.

Conclusions

It is concluded from this study that the observed deleterious effect of disorder-to-order transformation on the corrosion resistance of Ni₄Mo alloy is not caused by the process of atomic order itself. Instead, this behavior is correlated with changes in morphology of the ordered microstructure

caused by self-generated recrystallization to relieve the strain associated with continued growth of the ordered crystals. This involves a discontinuous reaction at grain boundaries leading to the formation of Mo-depleted zones degrading the resistance to intergranular corrosion attack. However, doping with Y is found to maintain an ultrafine ordered microstructure suppressing the occurrence of self-generated recrystallization and, therefore, improving the corrosion resistance of the Ni₄Mo alloy in the ordered condition.

Acknowledgment It is a pleasure to acknowledge the continued support of King Fahd University of Petroleum and Minerals.

References

1. F.G. Hodge, Nickel and high nickel alloys, in *Corrosion and Corrosion Protection Handbook*, ed. by P.A. Schweitzer (Marcel Dekker, New York, 1983), pp. 65–69
2. W.Z. Friend, *Corrosion of Nickel and Nickel-Base Alloys* (Wiley Interscience, New York, 1980), pp. 248–291
3. H.H. Uhlig, *Corrosion and Corrosion Control*, 2nd edn. (Wiley, New York, 1971), pp. 354–356
4. H.M. Tawancy, Long-range ordering behavior and mechanical properties of Ni–Mo-based alloys. *J. Mater. Sci.* **30**, 522–537 (1995)
5. C.R. Brooks, J.E. Spuriell, E.E. Stansbury, Physical metallurgy of Ni–Mo alloys. *Int. Met. Rev.* **2**, 210–248 (1984)
6. X.Y. Cheng, W.Q. Liu, Q. Li, The mechanism of order-induced intrinsic embrittlement in a stoichiometric Ni₄Mo alloy by TEM and 3DAP. *Mater. Sci. Eng., A* **486**, 177–182 (2008)
7. H.M. Tawancy, Mechanism of order-induced embrittlement in Ni–Ni₄Mo alloys. *J. Mater. Sci.* **26**, 3955–3963 (1991)
8. H.M. Tawancy, Comparative corrosion behavior of Ni–Mo and Ni–Mo–Cr alloys for applications in reducing environments. *J. Mater. Sci.* **41**, 8359–8362 (2006)
9. H.M. Tawancy, Corrosion-Resistant Nickel-Base Alloys, United States Patent No. 7,922,969 (2011)
10. H.M. Tawancy, M.O. Aboelfotoh, Yttrium-doped nanocrystalline Ni₄Mo: ultrahigh strength and high ductility combined with useful intermetallic properties. *J. Mater. Sci.* **45**, 3413–3418 (2010)
11. M.D. Nguyen, V. Vitek, A.P. Horsfield, Environmental dependence of bonding: A challenge for modelling intermetallics. *Prog. Mater. Sci.* **52**, 255–298 (2007)
12. T.V. Svistunova, Corrosion-resistant alloys for very highly corrosive media. *Met. Sci. Heat Treatment* **47**, 383–389 (2005)
13. Annual Book of ASTM Standards, G1-88: Standard Practice for Preparing, Cleaning, and Evaluating Corrosion Test Specimens vol. 03.02. (ASTM International, Materials Park, 2011)
14. M.G. Fontana, N.D. Green, *Corrosion Engineering* (McGraw Hill, New York, 1978), pp. 10–12
15. H.M. Tawancy, Formation of the DO₂₂-type superlattice during long-range ordering to Ni₄Mo in a Ni–Mo alloy. *Scripta Mater.* **18**, 343–346 (1998)
16. P.R. Okamoto, G. Thomas, Short-range order and micro-domains in Ni₄Mo system. *Acta Metall.* **19**, 825–827 (1971)
17. J.P. Chevalier, W.M. Stobbs, Short-range order and disorder-order transformation in stoichiometric Ni₄Mo. *Acta Metall.* **27**, 1197–1217 (1979)
18. L.E. Tanner, H.J. Leamy, Microstructure of order-disorder transitions, in *Order-Disorder Transformation in Metals*, ed. by H. Warlimont (Springer, Berlin, 1974), pp. 180–221